Title

The FIRE biosensor illuminates iron regulatory protein activity and cellular iron homeostasis

Journal

Cell Reports Methods, 5(1)

ISSN

2667-2375

Author

Sangokoya, Carolyn

Publication Date

2025

DOI

10.1016/j.crmeth.2024.100960

Cell Reports
Methods

Report

The FIRE biosensor illuminates iron regulatory protein activity and cellular iron homeostasis

Graphical abstract

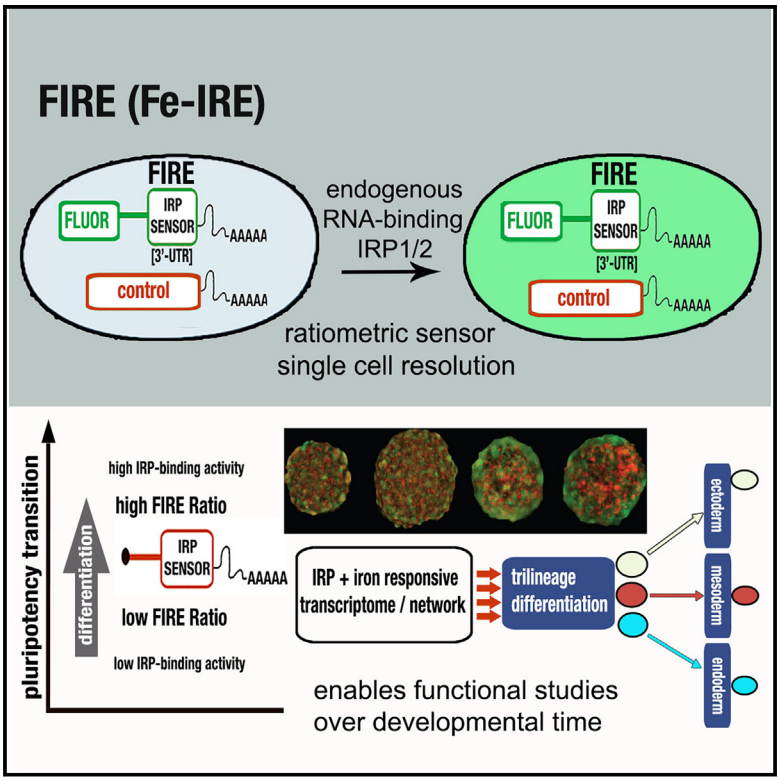

Highlights

- Fe-IRE (FIRE), a ratiometric dual biosensor of IRP activity and cellular iron status
- FIRE illuminates the timeline of IRP activity during pluripotent stem cell differentiation
- mFerrix-IRP lists iron/IRP-responsive transcripts in the context of early development
- FIRE advances functional studies of cellular iron homeostasis at single-cell resolution

Authors

Carolyn Sangokoya

Correspondence

carolyn.sangokoya@ucsf.edu

In brief

Iron is essential for life, yet the full context of its regulation in shaping cell fates in stem cells of the early developing mammalian embryo is not well understood. Sangokoya reports a ratiometric biosensor of iron regulatory protein (IRP) activity and cellular iron to advance functional studies at single-cell resolution.

Sangokoya, 2025, Cell Reports Methods *5*, 100960
January 27, 2025
https://doi.org/10.1016/j.crmeth.2024.100960

CellPress

Cell Reports Methods

CellPress
OPEN ACCESS

Report

The FIRE biosensor illuminates iron regulatory protein activity and cellular iron homeostasis

Carolyn Sangokoya[1,2,3,*]
[1]Department of Pathology, University of California, San Francisco, San Francisco, CA, USA
[2]The Eli and Edythe Broad Center of Regeneration Medicine and Stem Cell Research, University of California, San Francisco, San Francisco, CA, USA
[3]Lead contact
*Correspondence: carolyn.sangokoya@ucsf.edu
https://doi.org/10.1016/j.crmeth.2024.100960

MOTIVATION Little is known about how cellular iron regulation shapes cell fate, function, and plasticity, due in part to the lack of experimental systems that specifically and simultaneously sense, interrogate, and track iron regulatory protein (IRP) activity and iron metabolism. To develop a tractable method to follow iron-responsive metabolic changes during mammalian development, we engineered a ratiometric genetically encoded dual biosensor called FIRE (Fe-IRE [iron-responsive element]) that senses IRP activity and cellular iron status.

SUMMARY

On Earth, iron is abundant, bioavailable, and crucial for initiating the first catalytic reactions of life from prokaryotes to plants to mammals. Iron-complexed proteins are critical to biological pathways and essential cellular functions. While it is well known that the regulation of iron is necessary for mammalian development, little is known about the timeline of how specific transcripts network and interact in response to cellular iron regulation to shape cell fate, function, and plasticity in the developing embryo and beyond. Here, we present a ratiometric genetically encoded dual biosensor called FIRE (Fe-IRE [iron-responsive element]) to evaluate iron regulatory protein (IRP)-binding activity and cellular iron status in live cells, allowing for the study and dissection of dynamic changes in cellular iron and IRP activity over developmental time. FIRE reveals a previously unrecognized foundational timeline of IRP activity and cellular iron homeostasis during stem cell pluripotency transition and early differentiation.

INTRODUCTION

On Earth, iron is abundant, bioavailable, and crucial for initiating the first catalytic reactions of life from prokaryotes to plants to mammals.[1,2] At least 2% of human proteins include iron complexed within heme porphyrin rings, iron-sulfur clusters, or directly bound to proteins. These proteins are essential for most cellular functions, including ATP generation, DNA metabolism, mitochondrial function, and oxygen transport.[3,4] Iron's capacity to hold ferrous (Fe2+) and ferric (Fe3+) states make it essential for homeostatic plasticity across biological systems. To ensure proper cellular iron homeostasis, highly orchestrated regulation is required, as dysregulation can lead to iron toxicity, deficiency, cellular damage and death due to oxygen radicals and the Fenton reaction, disruption of protein function, and ferroptosis.[5] Dysregulation in iron balance is detrimental to human health, as iron overload results in an increased risk for chronic conditions, including diabetes and chronic liver disease, while iron deficiency remains among the top ten leading causes of disability worldwide, especially in women of childbearing age and young children.[6]

Studies in animal models and patients reveal that the activity of iron regulatory proteins (IRPs) are critical for iron homeostasis,[4,7] and the double loss of IRP1 and IRP2 results in embryonic lethality.[8,9] While mice with systemic deficiency of either of the two IRPs remain fertile and viable,[10] targeted deletions of IRP1 and IRP2 demonstrate that IRPs are the main physiologic iron sensors in mammals.[11] While the two IRPs are, to some extent, functionally redundant, IRP2 function predominates for iron homeostasis.[12] Systemic deletion of IRP2 in mice leads to anemia, diabetes, neurological symptoms, and defects in granulocyte development.[9,13,14] Consistent with these findings, biallelic loss of IRP2 has been shown to lead to human clinical and cellular phenotypes recapitulating the abnormalities in IRP2-deficient mice.[15]

As RNA-binding proteins, IRPs are differentially regulated. In iron-abundant conditions, the iron-responsive element (IRE)-binding site of IRP1 is blocked by an iron-sulfur cluster, but under iron-depleted conditions, disassembly of this cluster enables the RNA binding by IRP1. In contrast, under iron-abundant conditions, IRP2 is subject to post-translational ubiquitin-dependent degradation through the FBXL5 iron-responsive E3 ligase,[16,17] but in

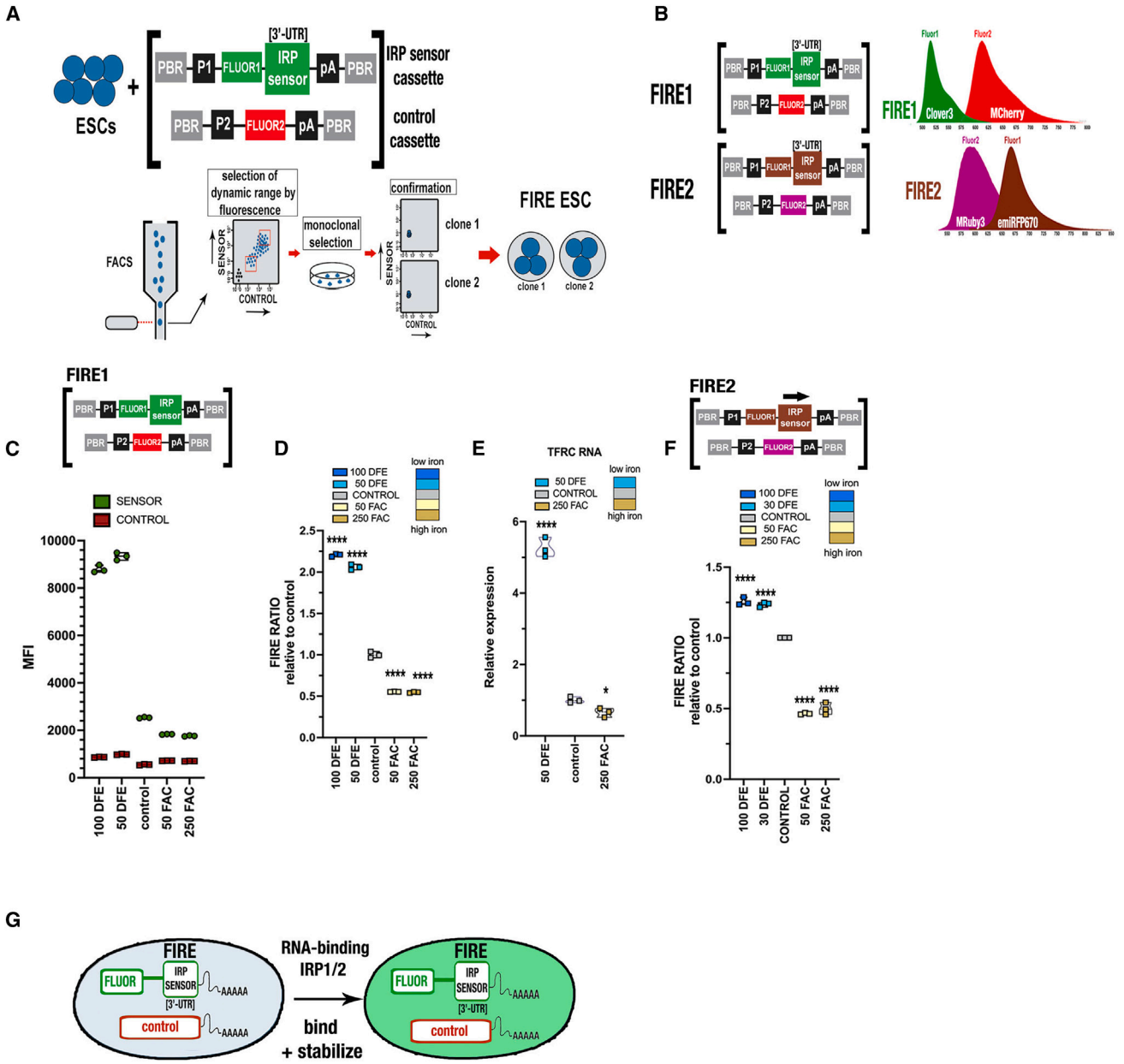

Figure 1. The FIRE sensor is a ratiometric dual biosensor of IRP activity and cellular iron status

(A) Schematic map organization of Fe-IRE (FIRE) biosensor showing the IRP sensor cassette and control cassette (top) diagram of the workflow from transfected embryonic stem cells (ESCs) to selection by fluorescence-activated cell sorting (FACS), monoclonal selection, and confirmation of clonality by flow cytometry (bottom). PBR, piggybac transposon repeat sequence; P1/P2, promoter; FLUOR, fluorescent protein open reading frame; pA, poly-adenylation sequence.

(B) Schematic map organization of FIRE1 (mClover3-sensor, mCherry-control) and FIRE2 (emiRFP670-sensor, mRuby3-control) on the left and images depicting respective emission spectra on the right.

(C) Schematic for FIRE1 (top). Iron gradient assay using deferoxamine (DFE), ferric ammonium citrate (FAC), and untreated condition. The median fluorescence intensity of FIRE1 sensor and control per experiment is shown (n = 3). Biological replicates are shown.

(D) FIRE ratios (sensor to control intensity values) measured per experiment (n = 3) shown in (C). Biological replicates are shown. Error bars represent SEM. ****p < 0.0001, unpaired two-tailed t test.

(E) Expression analysis of transferrin receptor (*Tfrc*) by qPCR in untreated control and after treatment with indicated DFE concentration and FAC concentration. The samples were collected for analysis in parallel with the data shown in (C) and (D). Biological replicates are shown. Error bars represent SEM. *p < 0.05 and ****p < 0.0001, unpaired two-tailed t test.

(legend continued on next page)

iron-depleted conditions, IRP2 is stabilized and acts as an RNA-binding protein. Thus, both IRPs function as RNA-binding proteins in similar conditions, and this IRP-IRE binding can also be influenced by environmental cues, including nitric oxide, hypoxia, and oxidative stress, in a cell context-dependent manner.[18]

At the cellular level, the import, export, utilization, and storage of iron are orchestrated by interactions between the IRPs and their target IREs in the untranslated regions (UTRs) of messenger RNA (mRNA). The IRP-IRE interactions function to regulate mRNA translation or stability, typically depending on the location of the IRE within the 5′ UTR or 3′ UTR. As targets of these RNA-binding proteins, a core group of mRNAs with known IREs encode key drivers of iron homeostasis. When iron is depleted, IRPs bind to the 5′ UTR IRE of mRNAs encoding ferritin iron storage proteins (FTH1, FTL1), the iron exporter ferroportin (SLC40A1), and the initial enzyme of heme biosynthesis erythroid 5-aminolevulininate synthase (ALAS2) to block translation[19] and thus limit iron storage, export, and excess utilization. In contrast, IRPs bind to the 3′ UTR IREs on the transferrin receptor mRNA. This 3′ UTR binding promotes the stability of transferrin receptor (TFRC) mRNA by protecting the mRNA from degradation by nucleases Regnase1[20] and Roquin-1,[21] resulting in increased transferrin receptor levels and cellular iron uptake.

Although cellular iron regulation is essential for embryonic development,[7–12,22–28] the essential IRP regulatory networks during embryonic development are not well understood precisely because maintaining the proper balance of iron is so essential. Emerging evidence suggests that the IRP regulome may extend beyond erythropoiesis, red blood cells, and even iron metabolism.[13,14,29] Until now, we have lacked experimental systems that specifically and simultaneously sense, interrogate, and track how IRP activity and cellular iron metabolism impact the mammalian organism at molecular, cellular, and spatial levels. The overarching biological functions of the IRP/IRE regulatory network in the post-implantation to peri-gastrulation embryo remain to be defined. We recently developed a ratiometric genetically encoded dual biosensor called FIRE (Fe-IRE) to evaluate IRP-binding activity and cellular iron status in live cells. Here, we report the FIRE sensor as a dual biosensor for IRP activity and cellular iron status. This study unveils and demonstrates that the FIRE sensor functions in mammalian embryonic stem cells (ESCs) and reveals a previously unrecognized initial timeline of IRP activity and cellular iron homeostasis during the homogeneous naive-to-formative state stem cell pluripotency transition toward early heterogeneous trilineage cell fates.

RESULTS

The FIRE sensor is a dual biosensor for IRP activity and cellular iron status

To engineer the FIRE sensor, two separate cassettes (sensor and control) were generated, each encoding a synthetic gene composed of a fluorescent protein driven by a ubiquitous mammalian promoter and punctuated by a poly-adenylation region. Each cassette is flanked on both sides by *piggy-bac* transposon regions. The IRP sensor cassette contains mammalian IRP-binding sites within the synthetic 3′ UTR following the stop codon of the fluorescent protein, putting this cassette under post-transcriptional regulation of the sensor cassette, while the control cassette features ubiquitous expression of a different fluorescent protein without any additional 3′ UTR regulation. The integration of the two cassettes by plasmid-based transfection into mouse ESCs followed by flow cytometry allows for sensitive selection of the desired dynamic range of ratiometric expression of the sensor to control fluorescence in transfected cells. Flow sorting and monoclonal selection, followed by additional cytometric confirmation, leads to the generation of multiple FIRE ESC clones (Figure 1A). Fluorescent protein combinations have been incorporated into this system to generate FIRE1 (mClover3-sensor, mCherry-control) and FIRE2 (emiRFP670-sensor, mRuby3-control) (Figure 1B).

To test the response of these FIRE-encoded cells in iron-deplete and iron-replete conditions, the cells were subject to an iron gradient by short-term iron chelation or addition and then assayed for fluorescence by flow cytometry. The generated FIRE ratios (sensor to control fluorescence intensities) under increasing gradients of iron chelation (low-iron condition) in FIRE1 ESCs demonstrated significantly higher FIRE ratios (Figures 1C, 1D, and S1) compared to untreated control conditions. In contrast, increasing gradients of exogenous iron (high-iron condition) in the FIRE ESCs demonstrated significantly lower FIRE ratios relative to untreated control cells (Figures 1C, 1D, and S1). To test the capability of IRP activity on endogenous targets despite the ubiquitous presence of the FIRE sensor in these cells, a subset of the FIRE1 ESCs were assayed for RNA expression of transferrin receptor (TFRC) by real-time qPCR. Increased TFRC RNA expression was seen in the low-iron condition (indicating IRP-driven stability) and decreased levels were seen in the high-iron condition, consistent with the loss of endogenous IRP activity, a known effect on TFRC transcripts with known 3′ UTR regulation by IRPs (Figure 1E). To test our FIRE2 cells, these were subjected to the same iron gradient (Figure 1F) and showed similar results to those of FIRE1, with FIRE ratios elevated in the low-iron condition and decreased in the high-iron condition relative to untreated. We then generated FIRE2-FLIP cells by flipping the IRP sensor sequence within its cassette and transfecting with the control cassette. Surprisingly, in low-iron conditions, FIRE2-FLIP cells demonstrated significantly *lower* FIRE ratios relative to untreated control cells and higher FIRE ratios in high-iron conditions with a mirror-image opposite effect (decreased in low-iron condition, stable or increased in high-iron condition) compared to FIRE2. This directionality of the FIRE sensor appears to be necessary for the stabilization effect (Figure S1). Endogenous IRP binding to the IRP sensor stabilizes and increases expression of the FIRE fluorescent protein transcript and subsequently the

(F) Schematic for FIRE2 (top). Iron gradient assay using DFE, FAC, and untreated condition. FIRE ratios (sensor to control intensity values) were measured per experiment ($n = 3$). Biological replicates are shown. Error bars represent SEM. ****$p < 0.0001$, unpaired two-tailed t test.

(G) Schematic of cell with FIRE ratiometric sensor without (left) and with (right) IRP binding activity to stabilize the sensor transcript and increase illumination of the FIRE sensor fluorescent protein.

See also Figure S1.

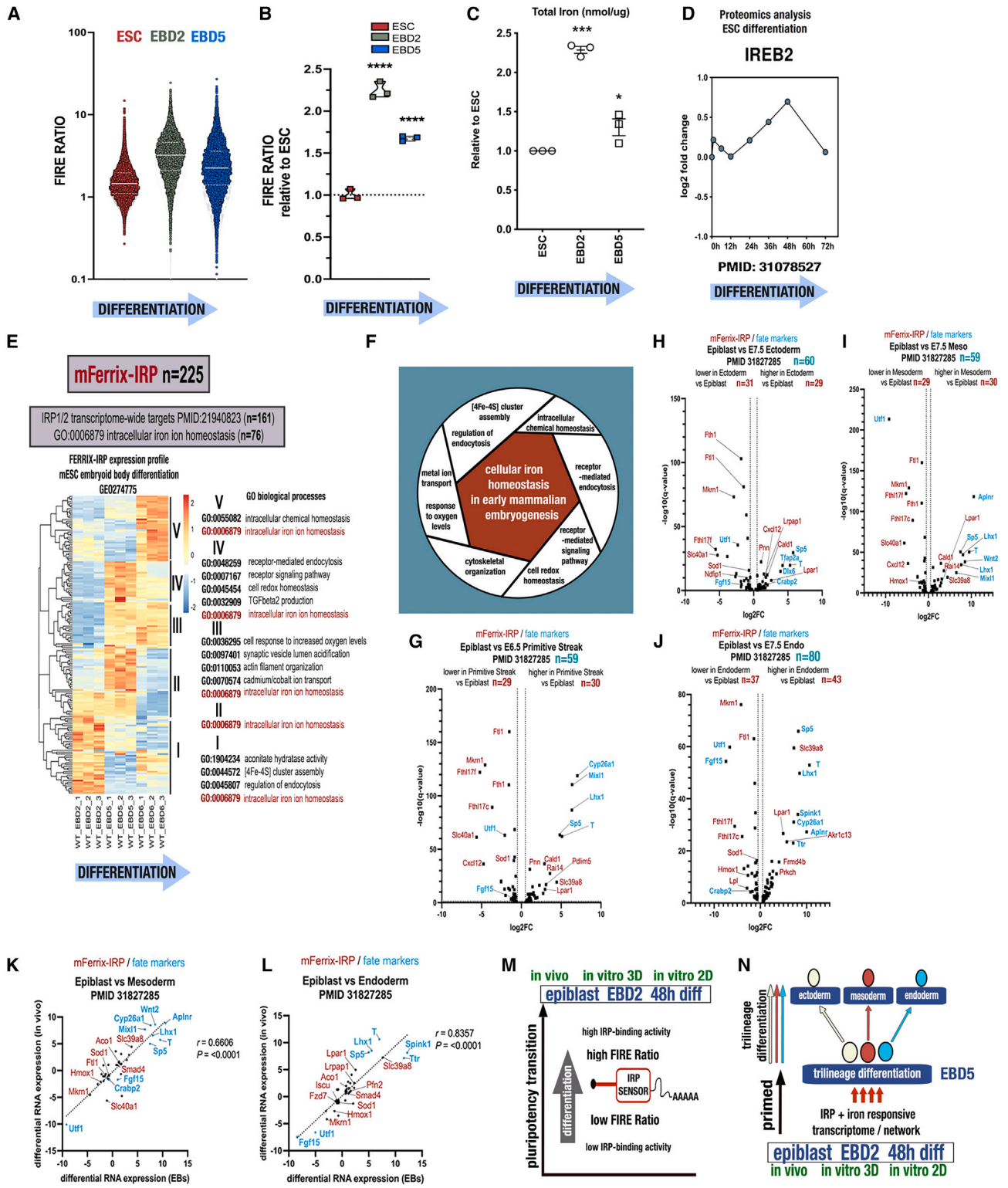

Figure 2. FIRE identifies timeline of IRP activity and cellular iron status during early ESC differentiation

(A) Flow cytometry analysis of FIRE1 ESCs and embryoid bodies (EBs) at EBD2 and EBD5. FIRE ratios (sensor to control intensity values) were measured per cell (ESC n = 29,567, EBD2 n = 15,208, EBD5 n = 10,948). Biological replicates are shown for n = 3 experiments.

(legend continued on next page)

fluorescence readout, allowing for the ratiometric FIRE ratio per cell (Figure 1G).

FIRE illuminates IRP activity during stem cell pluripotency transition and early differentiation

To characterize the impact of IRP activity during ESC differentiation and trilineage differentiation, we performed embryoid body (EB) differentiation of FIRE ESCs to EBD2 (formative state) and EBD5 (emergence of trilineage differentiation), with FIRE ratio analysis done by flow cytometry at single-cell resolution (Figures 2A, 2B, and S2A). At the ESC pluripotency state and pluripotency transition to EBD2 (epiblast-like) stage of differentiation, the cells are still a relatively homogeneous population at the transcriptomic level,[30,31] and we uncover a peak in the FIRE ratio at EBD2. By EBD5, we identify decreased FIRE ratios with increased dispersion, indicating an increased range of IRP activity and cellular iron status in this slightly more differentiated population during early trilineage differentiation.

To measure the total (ferrous Fe2+ and ferric Fe3+) iron in ESCs and EBs over the course of EB differentiation, a ferrozine-based assay[32] was performed and showed a similar peak of significantly increased total iron at EBD2 (Figure 2C). Proteomic analysis of IRP2 (*Ireb2*) indicates an initial peak at 48 h of differentiation, syncing with the formative pluripotency state and EBD2. These orthogonal data demonstrate a peak of IRP2 protein at the same time—during the EBD2 epiblast-like state—that the FIRE sensor indicates high IRP activity as well as high total cellular iron relative to ESCs (Figure 2D).

To generate a list of potential IRP transcript targets in pluripotent stem cells, we combined transcripts known to play a role in cellular iron ion homeostasis (GO: 0006879) with those reported in studies of IRP transcriptome-wide targets in later stages of mouse development and in the adult mammalian cells and tissues.[29] We called this the mFerrix-IRP list (225 genes, listed in Table S1).

To characterize the expression profile of these mFerrix-IRP RNA transcripts in mouse EBs during the epiblast-like state through trilineage differentiation, we evaluated the expression of these 225 transcripts in EBs differentiated to EBD2, EBD5, and EBD6. Of these, 168 transcripts were differentially expressed in mouse EBs in this study or identified in *in vivo* mouse embryo datasets[30,31] as specifically differentially expressed in epiblast versus ectoderm, mesoderm, or endoderm (Figures 2E and S2B–S2F). Five groups of transcripts (I–V) with similar expression changes from EBD2 to EBD5 and EBD6 were identified by transcriptomic analysis, heatmap visualization, and Gene Ontology analysis. These groups include those that play roles in the regulation of endocytosis, iron-sulfur cluster assembly, metal ion transport, cytoskeletal organization, cell response to oxygen levels, cell redox homeostasis, receptor-mediated signaling pathways, transforming growth factor beta2 (TGF-β2) production, intracellular chemical homeostasis, and intracellular iron ion homeostasis (Figure 2F). Remarkably, the first group (I) indicates basic iron-related cellular impacts followed by more integrated categories, from response to metabolic and environmental homeostasis (groups II and III) to redox homeostasis, endocytosis, and signaling pathways (group IV) to more general chemical homeostasis (group V) (Figures S2B–S2F).

We subsequently evaluated the mFerrix-IRP list for differential expression ($p < 0.05$, false discovery rate [FDR] < 0.05) within published single-cell RNA transcriptomic datasets of mouse embryo *in vivo* transitions between epiblast to the embryonic day (E) 6.5 primitive streak ($n = 59$; 30 up, 29 down) (Figure 2G), E7.5 ectoderm ($n = 60$; 29 up, 31 down) (Figure 2H), E7.5 mesoderm ($n = 59$; 30 up, 29 down) (Figure 2I), and E7.5 endoderm ($n = 80$; 43 up, 37 down) (Figure 2J).[30] These data indicate the relatively higher expression of iron storage protein transcripts (*Ftl1*, *Fth1*, *Fthl17f*, *Fthl17c*) at the epiblast stage compared to primitive streak (Figure 2G) and to further lineage commitment to ectoderm (Figure 2H), mesoderm (Figure 2I), and endoderm (Figure 2J). We find these embryonic epiblast data to be consistent with the increased total iron in the *in vitro* EBD2/epiblast-like cells (Figure 2C). Additionally from single-cell RNA transcriptomic datasets,[30] we identified consistent differential expression of mFerrix-IRP transcripts between *in vivo* and EB model data[30] during the epiblast-to-mesoderm (Figure 2K) and epiblast-to-endoderm transitions (Figure 2L).

Using this FIRE sensor, we identify early IRP activity that peaks at the epiblast-like stage of ESC pluripotency transition and demonstrates distributed, more heterogeneous FIRE ratios corresponding with the heterogeneous population in early trilineage differentiation. The FIRE sensor will allow for distinct dissection of IRP/iron-responsive transcripts during trilineage differentiation in early embryogenesis (Figures 2M and 2N).

(B) FIRE ratios (sensor to control intensity values) measured per experiment ($n = 3$) shown in (A). Biological replicates are shown. Error bars represent SEM. ****$p < 0.0001$, unpaired two-tailed t test.
(C) Total (ferrous Fe2+ and ferric Fe3+) iron measured by ferrozine-based assay in ESCs and EBs over the course of EB differentiation. Biological replicates are shown. Error bars represent SEM. *$p < 0.05$ and ***$p < 0.001$, unpaired two-tailed t test.
(D) Proteomics analysis by log2 fold change of IREB2 (IRP2) during ESC differentiation (PMID: 31078527) from 0 to 72 h.
(E) (Top) mFerrix-IRP description. (Middle) Heatmap display of RNA sequencing (RNA-seq) expression data of wild-type mouse EBD2, EBD5, and EBD6 EBs established by RNA-seq over three experiments ($n = 3$). An mFerrix-IRP transcript subset of the original dataset is shown (168 transcripts) and is divided into sections by expression categories I–V. Biological replicates are shown. (Right) Gene Ontology (GO) categories amplified in expression categories.
(F) Schematic of top GO-based categories across mFerrix-IRP list during EB differentiation.
(G–J) Volcano plot of transcriptomic data from single-cell RNA-seq datasets of mouse embryo *in vivo* transitions between epiblast to the E6.5 primitive streak (G), E7.5 ectoderm (H), E7.5 mesoderm (I), and E7.5 endoderm (J).
(K and L) mFerrix-IRP subset of differential RNA expression in *in vivo* embryos compared to EBs from published dataset, including fate markers identified in that dataset.
(M) Schematic summary of FIRE ratio results from ESC to epiblast/EBD2/48 h differentiation assayed *in vivo* and *in vitro* in two (2D) and three dimensions (3D).
(N) Schematic summary of window of poorly understood IRP/iron-responsive transcriptome/network in early mammalian development.
See also Figure S2 and Table S1.

DISCUSSION

In mammals, the labile iron pool and cellular iron homeostasis must be carefully regulated due to the propensity of this pool to undergo spontaneous redox reactions, resulting in iron toxicity, deficiency, cellular damage and death due to oxygen radicals and the Fenton reaction, disruption of protein function, and ferroptosis.[5,33,34] The breadth of IRP-regulated transcriptomic networks and their cellular regulatory roles, specifically the essential IRP regulatory networks during embryonic development, are not well understood precisely because maintaining the proper balance of iron is so essential to viability. Thus, we have engineered a ratiometric genetically encoded dual biosensor to evaluate IRP-binding activity and cellular iron status in live cells over developmental time and enable the dissection of these networks.

Our findings highlight a relatively higher FIRE ratio during early stem cell differentiation to EBD2/epiblast-like cells. This demonstrates an iron-demanding state where the demonstrated IRP2 protein levels and IRP1/2 activity coincide with the accumulation of iron. This initial peak in IRP activity at the EBD2/epiblast-like cell (*in vitro*) corresponds to the epiblast/formative pluripotency state *in vivo.* At this same stage, the peak in total (ferrous + ferric) iron coincides with the high expression of iron storage transcripts that dissipates with lineage commitment. In this report, we compiled the mFerrix-IRP list of iron- and IRP-responsive transcripts identified in other contexts to comparatively highlight those differentially expressed during *in vitro* and *in vivo* mouse early embryonic development. Intriguingly, the targets of high IRP activity at and shortly after the epiblast stage likely play a role in the process of lineage commitment during primed pluripotency and may play more general roles in other plastic mammalian states in metabolic and lineage priming toward cell states and fates.

To date, the study of cellular iron homeostasis has relied on quantifying iron (total, ferric, or ferrous) through supplementation and chelation/sequestration experiments, and the development of fluorescent iron probes has significantly increased our ability to study both ferrous and ferric iron states with greater selectivity.[35–37] The approach to engineering FIRE cells by selecting a dynamic range prior to monoclonal selection allows for the ability to fully capture the range of IRP activity in the chosen cell type. FIRE1 and FIRE2 are offered as two versions of FIRE with different spectral ranges that can be used to multiplex with other fluorophores, sensors, or labeled antibodies/elements in mammalian cells. The addition of FIRE to this vast toolbox will enable new insights into the roles of IRP and cellular iron status in stem cell biology as well as in general biology/pathobiology in mammalian cells.

Our FIRE2-FLIP results show a mirror-image effect to gene regulation of the fluorophore gene when the sensor 3′ UTR sequence is flipped. In iron limitation, the sensor reports lower IRP binding instead of higher IRP binding. These results show "loss of binding" in an environment when IRP activity is expected to increase and thus demonstrate the potential effect of directional orientation of iron response elements. While deletional mutagenesis continues to be a powerful tool to discovery, this example can contribute to the further evolution of gene regulatory elements as tailored RNA switches for synthetic biology.

Finally, FIRE enables a deconvolution of parallel combinatorial actions of development specifically through the molecular and metabolic lens of cellular iron homeostasis. By leveraging the ability to multiplex analysis with other metabolic (i.e., lipid, calcium, other metals), cell cycle, or cell state (apoptosis, mechano-sensitive) phenotypes over developmental time, FIRE will allow for further illumination of iron-dependent phenotypes and their drivers in areas where labile iron flux plays critical roles—in cell signaling, energy metabolism, hypoxia- and oxygen-dependent changes in iron redox homeostasis, and ferroptosis and related cell death pathways. In combination with transcriptomics at spatial resolution, we will be better able to understand how iron-related genetic, molecular, environmental, and signaling perturbations regulate cell fates and states.

Limitations of the study

Limitations to FIRE at this time are that (1) it offers a single-cell-level cumulative readout, while selective probes can now localize to organelles and also report on ferric or ferrous iron states[38–41] and (2) it cannot distinguish the IRP1 and IRP2 binding activities. Despite these limitations, further genetic engineering to encode targeting motifs and multiplex with these existing selective probes could allow for an organellar lens as desired, and selective sensors in the future can allow for distinction between IRP1/2 binding. We expect that with FIRE, the opportunities to discover and dissect the IRP and iron-responsive transcriptomic and molecular-metabolic networks at single-cell resolution will increase not only in the developmental context but in a variety of mammalian cell types.

RESOURCE AVAILABILITY

Lead contact

All other information and resources supporting the findings of this study are available from the corresponding author upon request (carolyn.sangokoya@ucsf.edu).

Materials availability

Plasmids generated in this study have been deposited to Addgene.

Data and code availability

- Sequencing data that support the findings of this study have been deposited in the Gene Expression Omnibus (GEO)[42] and are publicly available as of the date of publication.
- Source data supporting this study have been deposited at Zenodo at Zenodo: https://doi.org/10.5281/zenodo.13932639 and are publicly available as of the date of publication.
- Plasmids generated in this study have been deposited at Addgene and are publicly available as of the date of publication.
- This paper does not report original code.
- Any additional information required to reanalyze the data reported in this paper is available from the lead contact upon request.

ACKNOWLEDGMENTS

Flow cytometry was performed at the UCSF Parnassus Flow Cytometry Core, supported in part by the DRC Center grant NIH P30 DK063720. Sequencing was performed at the UCSF Center for Advanced Technology, supported by UCSF PBBR, RRP IMIA, and NIH 1S10OD028511-01 grants. This research was supported by funding from NIH/NICHD (K08HD105017) (to C.S.) and the Burroughs Wellcome Fund (to C.S.).

AUTHOR CONTRIBUTIONS

C.S. developed the concept and designed the experiments, conducted all experiments, interpreted the data, and wrote and edited the manuscript.

DECLARATION OF INTERESTS

The author declares no competing interests.

STAR★METHODS

Detailed methods are provided in the online version of this paper and include the following:

- KEY RESOURCES TABLE
- EXPERIMENTAL MODEL AND STUDY PARTICIPANT DETAILS
  - ESC cell culture
- METHOD DETAILS
  - Construction and cloning of FIRE cassettes
  - Generation of FIRE ESCs
  - Cell culture and embryoid body generation and differentiation
  - Real-time qPCR
  - RNA-seq library preparation and sequencing
  - Bulk RNA-Seq data pre-processing and analysis
  - Gene ontology and GO enrichment analysis
  - Flow cytometry
- QUANTIFICATION AND STATISTICAL ANALYSIS

SUPPLEMENTAL INFORMATION

Supplemental information can be found online at https://doi.org/10.1016/j.crmeth.2024.100960.

Received: October 21, 2024
Revised: November 18, 2024
Accepted: December 20, 2024
Published: January 16, 2025

REFERENCES

1. Muchowska, K.B., Varma, S.J., and Moran, J. (2019). Synthesis and breakdown of universal metabolic precursors promoted by iron. Nature *569*, 104–107. https://doi.org/10.1038/s41586-019-1151-1.
2. Frey, P.A., and Reed, G.H. (2012). The ubiquity of iron. ACS Chem. Biol. *7*, 1477–1481. https://doi.org/10.1021/cb300323q.
3. Andreini, C., Putignano, V., Rosato, A., and Banci, L. (2018). The human iron-proteome. Metallomics *10*, 1223–1231. https://doi.org/10.1039/c8mt00146d.
4. Galy, B., Conrad, M., and Muckenthaler, M. (2024). Mechanisms controlling cellular and systemic iron homeostasis. Nat. Rev. Mol. Cell Biol. *25*, 133–155. https://doi.org/10.1038/s41580-023-00648-1.
5. Dixon, S.J., and Stockwell, B.R. (2014). The role of iron and reactive oxygen species in cell death. Nat. Chem. Biol. *10*, 9–17. https://doi.org/10.1038/nchembio.1416.
6. GBD 2021 Diseases and Injuries Collaborators (2024). Global incidence, prevalence, years lived with disability (YLDs), disability-adjusted life-years (DALYs), and healthy life expectancy (HALE) for 371 diseases and injuries in 204 countries and territories and 811 subnational locations, 1990-2021: a systematic analysis for the Global Burden of Disease Study 2021. Lancet *403*, 2133–2161. https://doi.org/10.1016/S0140-6736(24)00757-8.
7. Galy, B., Ferring-Appel, D., Kaden, S., Gröne, H.-J., and Hentze, M.W. (2008). Iron regulatory proteins are essential for intestinal function and control key iron absorption molecules in the duodenum. Cell Metabol. *7*, 79–85. https://doi.org/10.1016/j.cmet.2007.10.006.
8. Smith, S.R., Ghosh, M.C., Ollivierre-Wilson, H., Hang Tong, W., and Rouault, T.A. (2006). Complete loss of iron regulatory proteins 1 and 2 prevents viability of murine zygotes beyond the blastocyst stage of embryonic development. Blood Cells Mol. Dis. *36*, 283–287. https://doi.org/10.1016/j.bcmd.2005.12.006.
9. Wilkinson, N., and Pantopoulos, K. (2014). The IRP/IRE system in vivo: insights from mouse models. Front. Pharmacol. *5*, 176. https://doi.org/10.3389/fphar.2014.00176.
10. Galy, B., Ferring, D., Minana, B., Bell, O., Janser, H.G., Muckenthaler, M., Schümann, K., and Hentze, M.W. (2005). Altered body iron distribution and microcytosis in mice deficient in iron regulatory protein 2 (IRP2). Blood *106*, 2580–2589. https://doi.org/10.1182/blood-2005-04-1365.
11. Rouault, T.A. (2006). The role of iron regulatory proteins in mammalian iron homeostasis and disease. Nat. Chem. Biol. *2*, 406–414. https://doi.org/10.1038/nchembio807.
12. Meyron-Holtz, E.G., Ghosh, M.C., Iwai, K., LaVaute, T., Brazzolotto, X., Berger, U.V., Land, W., Ollivierre-Wilson, H., Grinberg, A., Love, P., and Rouault, T.A. (2004). Genetic ablations of iron regulatory proteins 1 and 2 reveal why iron regulatory protein 2 dominates iron homeostasis. EMBO J. *23*, 386–395. https://doi.org/10.1038/sj.emboj.7600041.
13. Santos, M.C.F.D., Anderson, C.P., Neschen, S., Zumbrennen-Bullough, K.B., Romney, S.J., Kahle-Stephan, M., Rathkolb, B., Gailus-Durner, V., Fuchs, H., Wolf, E., et al. (2020). Irp2 regulates insulin production through iron-mediated Cdkal1-catalyzed tRNA modification. Nat. Commun. *11*, 296. https://doi.org/10.1038/s41467-019-14004-5.
14. Bonadonna, M., Altamura, S., Tybl, E., Palais, G., Qatato, M., Polycarpou-Schwarz, M., Schneider, M., Kalk, C., Rüdiger, W., Ertl, A., et al. (2022). Iron regulatory protein (IRP)-mediated iron homeostasis is critical for neutrophil development and differentiation in the bone marrow. Sci. Adv. *8*, eabq4469. https://doi.org/10.1126/sciadv.abq4469.
15. Costain, G., Ghosh, M.C., Maio, N., Carnevale, A., Si, Y.C., Rouault, T.A., and Yoon, G. (2019). Absence of iron-responsive element-binding protein 2 causes a novel neurodegenerative syndrome. Brain *142*, 1195–1202. https://doi.org/10.1093/brain/awz072.
16. Salahudeen, A.A., Thompson, J.W., Ruiz, J.C., Ma, H.-W., Kinch, L.N., Li, Q., Grishin, N.V., and Bruick, R.K. (2009). An E3 ligase possessing an iron-responsive hemerythrin domain is a regulator of iron homeostasis. Science *326*, 722–726. https://doi.org/10.1126/science.1176326.
17. Vashisht, A.A., Zumbrennen, K.B., Huang, X., Powers, D.N., Durazo, A., Sun, D., Bhaskaran, N., Persson, A., Uhlen, M., Sangfelt, O., et al. (2009). Control of iron homeostasis by an iron-regulated ubiquitin ligase. Science *326*, 718–721. https://doi.org/10.1126/science.1176333.
18. Anderson, C.P., Shen, M., Eisenstein, R.S., and Leibold, E.A. (2012). Mammalian iron metabolism and its control by iron regulatory proteins. Biochim. Biophys. Acta *1823*, 1468–1483. https://doi.org/10.1016/j.bbamcr.2012.05.010.
19. Muckenthaler, M., Gray, N.K., and Hentze, M.W. (1998). IRP-1 binding to ferritin mRNA prevents the recruitment of the small ribosomal subunit by the cap-binding complex eIF4F. Mol. Cell. *2*, 383–388. https://doi.org/10.1016/s1097-2765(00)80282-8.
20. Yoshinaga, M., Nakatsuka, Y., Vandenbon, A., Ori, D., Uehata, T., Tsujimura, T., Suzuki, Y., Mino, T., and Takeuchi, O. (2017). Regnase-1 Maintains Iron Homeostasis via the Degradation of Transferrin Receptor 1 and Prolyl-Hydroxylase-Domain-Containing Protein 3 mRNAs. Cell Rep. *19*, 1614–1630. https://doi.org/10.1016/j.celrep.2017.05.009.
21. Corral, V.M., Schultz, E.R., Eisenstein, R.S., and Connell, G.J. (2021). Roquin is a major mediator of iron-regulated changes to transferrin receptor-1 mRNA stability. iScience *24*, 102360. https://doi.org/10.1016/j.isci.2021.102360.
22. Cooperman, S.S., Meyron-Holtz, E.G., Olivierre-Wilson, H., Ghosh, M.C., McConnell, J.P., and Rouault, T.A. (2005). Microcytic anemia, erythropoietic protoporphyria, and neurodegeneration in mice with targeted deletion of iron-regulatory protein 2. Blood *106*, 1084–1091. https://doi.org/10.1182/blood-2004-12-4703.

23. Galy, B., Ferring-Appel, D., Sauer, S.W., Kaden, S., Lyoumi, S., Puy, H., Kölker, S., Gröne, H.-J., and Hentze, M.W. (2010). Iron regulatory proteins secure mitochondrial iron sufficiency and function. Cell Metabol. *12*, 194–201. https://doi.org/10.1016/j.cmet.2010.06.007.

24. Ferring-Appel, D., Hentze, M.W., and Galy, B. (2009). Cell-autonomous and systemic context-dependent functions of iron regulatory protein 2 in mammalian iron metabolism. Blood *113*, 679–687. https://doi.org/10.1182/blood-2008-05-155093.

25. LaVaute, T., Smith, S., Cooperman, S., Iwai, K., Land, W., Meyron-Holtz, E., Drake, S.K., Miller, G., Abu-Asab, M., Tsokos, M., et al. (2001). Targeted deletion of the gene encoding iron regulatory protein-2 causes misregulation of iron metabolism and neurodegenerative disease in mice. Nat. Genet. *27*, 209–214. https://doi.org/10.1038/84859.

26. Galy, B., Ferring-Appel, D., Becker, C., Gretz, N., Gröne, H.-J., Schümann, K., and Hentze, M.W. (2013). Iron regulatory proteins control a mucosal block to intestinal iron absorption. Cell Rep. *3*, 844–857. https://doi.org/10.1016/j.celrep.2013.02.026.

27. Levy, J.E., Jin, O., Fujiwara, Y., Kuo, F., and Andrews, N.C. (1999). Transferrin receptor is necessary for development of erythrocytes and the nervous system. Nat. Genet. *21*, 396–399. https://doi.org/10.1038/7727.

28. Ned, R.M., Swat, W., and Andrews, N.C. (2003). Transferrin receptor 1 is differentially required in lymphocyte development. Blood *102*, 3711–3718. https://doi.org/10.1182/blood-2003-04-1086.

29. Sanchez, M., Galy, B., Schwanhaeusser, B., Blake, J., Bähr-Ivacevic, T., Benes, V., Selbach, M., Muckenthaler, M.U., and Hentze, M.W. (2011). Iron regulatory protein-1 and -2: transcriptome-wide definition of binding mRNAs and shaping of the cellular proteome by iron regulatory proteins. Blood *118*, e168–e179. https://doi.org/10.1182/blood-2011-04-343541.

30. Argelaguet, R., Clark, S.J., Mohammed, H., Stapel, L.C., Krueger, C., Kapourani, C.-A., Imaz-Rosshandler, I., Lohoff, T., Xiang, Y., Hanna, C.W., et al. (2019). Multi-omics profiling of mouse gastrulation at single-cell resolution. Nature *576*, 487–491. https://doi.org/10.1038/s41586-019-1825-8.

31. Yang, P., Humphrey, S.J., Cinghu, S., Pathania, R., Oldfield, A.J., Kumar, D., Perera, D., Yang, J.Y.H., James, D.E., Mann, M., and Jothi, R. (2019). Multi-omic Profiling Reveals Dynamics of the Phased Progression of Pluripotency. Cell Syst. *8*, 427–445.e10. https://doi.org/10.1016/j.cels.2019.03.012.

32. Riemer, J., Hoepken, H.H., Czerwinska, H., Robinson, S.R., and Dringen, R. (2004). Colorimetric ferrozine-based assay for the quantitation of iron in cultured cells. Anal. Biochem. *331*, 370–375. https://doi.org/10.1016/j.ab.2004.03.049.

33. Aisen, P., Enns, C., and Wessling-Resnick, M. (2001). Chemistry and biology of eukaryotic iron metabolism. Int. J. Biochem. Cell Biol. *33*, 940–959. https://doi.org/10.1016/s1357-2725(01)00063-2.

34. Sies, H., and Jones, D.P. (2020). Reactive oxygen species (ROS) as pleiotropic physiological signalling agents. Nat. Rev. Mol. Cell Biol. *21*, 363–383. https://doi.org/10.1038/s41580-020-0230-3.

35. Gonciarz, R.L., Collisson, E.A., and Renslo, A.R. (2021). Ferrous Iron-Dependent Pharmacology. Trends Pharmacol. Sci. *42*, 7–18. https://doi.org/10.1016/j.tips.2020.11.003.

36. Aron, A.T., Reeves, A.G., and Chang, C.J. (2018). Activity-based sensing fluorescent probes for iron in biological systems. Curr. Opin. Chem. Biol. *43*, 113–118. https://doi.org/10.1016/j.cbpa.2017.12.010.

37. Aron, A.T., Heffern, M.C., Lonergan, Z.R., Vander Wal, M.N., Blank, B.R., Spangler, B., Zhang, Y., Park, H.M., Stahl, A., Renslo, A.R., et al. (2017). In vivo bioluminescence imaging of labile iron accumulation in a murine model of Acinetobacter baumannii infection. Proc. Natl. Acad. Sci. USA *114*, 12669–12674. https://doi.org/10.1073/pnas.1708747114.

38. Niwa, M., Hirayama, T., Okuda, K., and Nagasawa, H. (2014). A new class of high-contrast Fe(II) selective fluorescent probes based on spirocyclized scaffolds for visualization of intracellular labile iron delivered by transferrin. Org. Biomol. Chem. *12*, 6590–6597. https://doi.org/10.1039/c4ob00935e.

39. Hirayama, T., Tsuboi, H., Niwa, M., Miki, A., Kadota, S., Ikeshita, Y., Okuda, K., and Nagasawa, H. (2017). A universal fluorogenic switch for Fe(ii) ion based on N-oxide chemistry permits the visualization of intracellular redox equilibrium shift towards labile iron in hypoxic tumor cells. Chem. Sci. *8*, 4858–4866. https://doi.org/10.1039/c6sc05457a.

40. Niwa, M., Hirayama, T., Oomoto, I., Wang, D.O., and Nagasawa, H. (2018). Fe(II) Ion Release during Endocytotic Uptake of Iron Visualized by a Membrane-Anchoring Fe(II) Fluorescent Probe. ACS Chem. Biol. *13*, 1853–1861. https://doi.org/10.1021/acschembio.7b00939.

41. Hirayama, T., Miki, A., and Nagasawa, H. (2019). Organelle-specific analysis of labile Fe(ii) during ferroptosis by using a cocktail of various colour organelle-targeted fluorescent probes. Metallomics *11*, 111–117. https://doi.org/10.1039/c8mt00212f.

42. Edgar, R., Domrachev, M., and Lash, A.E. (2002). Gene Expression Omnibus: NCBI gene expression and hybridization array data repository. Nucleic Acids Res. *30*, 207–210. https://doi.org/10.1093/nar/30.1.207.

43. Bajar, B.T., Wang, E.S., Lam, A.J., Kim, B.B., Jacobs, C.L., Howe, E.S., Davidson, M.W., Lin, M.Z., and Chu, J. (2016). Improving brightness and photostability of green and red fluorescent proteins for live cell imaging and FRET reporting. Sci. Rep. *6*, 20889. https://doi.org/10.1038/srep20889.

44. Casey, J.L., Hentze, M.W., Koeller, D.M., Caughman, S.W., Rouault, T.A., Klausner, R.D., and Harford, J.B. (1988). Iron-responsive elements: regulatory RNA sequences that control mRNA levels and translation. Science *240*, 924–928. https://doi.org/10.1126/science.2452485.

45. Casey, J.L., Koeller, D.M., Ramin, V.C., Klausner, R.D., and Harford, J.B. (1989). Iron regulation of transferrin receptor mRNA levels requires iron-responsive elements and a rapid turnover determinant in the 3' untranslated region of the mRNA. EMBO J. *8*, 3693–3699. https://doi.org/10.1002/j.1460-2075.1989.tb08544.x.

46. Shaner, N.C., Campbell, R.E., Steinbach, P.A., Giepmans, B.N.G., Palmer, A.E., and Tsien, R.Y. (2004). Improved monomeric red, orange and yellow fluorescent proteins derived from Discosoma sp. red fluorescent protein. Nat. Biotechnol. *22*, 1567–1572. https://doi.org/10.1038/nbt1037.

47. Matlashov, M.E., Shcherbakova, D.M., Alvelid, J., Baloban, M., Pennacchietti, F., Shemetov, A.A., Testa, I., and Verkhusha, V.V. (2020). A set of monomeric near-infrared fluorescent proteins for multicolor imaging across scales. Nat. Commun. *11*, 239. https://doi.org/10.1038/s41467-019-13897-6.

48. Dobin, A., Davis, C.A., Schlesinger, F., Drenkow, J., Zaleski, C., Jha, S., Batut, P., Chaisson, M., and Gingeras, T.R. (2013). STAR: ultrafast universal RNA-seq aligner. Bioinformatics *29*, 15–21. https://doi.org/10.1093/bioinformatics/bts635.

49. Li, B., and Dewey, C.N. (2011). RSEM: accurate transcript quantification from RNA-Seq data with or without a reference genome. BMC Bioinf. *12*, 323. https://doi.org/10.1186/1471-2105-12-323.

50. Robinson, M.D., McCarthy, D.J., and Smyth, G.K. (2010). edgeR: a Bioconductor package for differential expression analysis of digital gene expression data. Bioinformatics *26*, 139–140. https://doi.org/10.1093/bioinformatics/btp616.

51. Love, M.I., Huber, W., and Anders, S. (2014). Moderated estimation of fold change and dispersion for RNA-seq data with DESeq2. Genome Biol. *15*, 550. https://doi.org/10.1186/s13059-014-0550-8.

52. Ashburner, M., Ball, C.A., Blake, J.A., Botstein, D., Butler, H., Cherry, J.M., Davis, A.P., Dolinski, K., Dwight, S.S., Eppig, J.T., et al. (2000). Gene Ontology: Tool for the unification of biology. Nat. Genet. *25*, 25–29. https://doi.org/10.1038/75556.

53. Thomas, P.D., Ebert, D., Muruganujan, A., Mushayahama, T., Albou, L.-P., and Mi, H. (2022). PANTHER: Making genome-scale phylogenetics accessible to all. Protein Sci. *31*, 8–22. https://doi.org/10.1002/pro.4218.

CellPress
OPEN ACCESS

STAR★METHODS

KEY RESOURCES TABLE

REAGENT or RESOURCE	SOURCE	IDENTIFIER
Chemicals, peptides, and recombinant proteins		
Deferoxamine Mesylate	Emd Millipore	CAS Number: 138-14-7
Ferric Ammonium Citrate	Spectrum Chemical	CAS Number: 1185-57-5
2i (PD0325901 and CHIR99021)	Axon MedChem	Axon: 2128
LIF Leukemia inhibitory factor	MilliporeSigma	MilliporeSigma: ESG1107
Fugene6	Promega	Promega: E2691
Critical commercial assays		
KAPA RNA Hyperprep kit (cDNA library generation)	Roche	Roche: KK8541
Deposited data		
Raw and analyzed data	This paper	GEO: GSE274775
Source data	This paper	https://doi.org/10.5281/zenodo.13932639
Experimental models: Cell lines		
Mouse: V6.5 mouse embryonic stem cells	Laboratory of Robert Blelloch	RRID:CVCL_C865
Oligonucleotides		
qPCR Primer: Tfrc Forward: AAATTCC CCGTTGTTGAGGC Reverse: TGATGACTGAGATGGCGGAA	This paper	N/A
Recombinant DNA		
Plasmid: FIRES-PBCS-CLV3	This paper	Addgene 228697
Plasmid: FIREC-PBCS-MC2	This paper	Addgene 228698
Plasmid: FIRES-PBCS-E670	This paper	Addgene 228699
Plasmid: FIRES-FLIP-PBCS-E670	This paper	Addgene 228701
Plasmid: FIREC-PBCS-MR3	This paper	Addgene 228700

EXPERIMENTAL MODEL AND STUDY PARTICIPANT DETAILS

ESC cell culture

V6.5 mouse ESCs (RRID:CVCL_C865) derived from the F1 hybrid of 129SvJae/C57BL/6 were grown and maintained at 37C and 5% CO2 on 0.2% gelatin-coated plates, cultured in ESC medium (custom DMEM) supplemented with 15% FBS (Corning Mediatech), LIF (1000U/mL, custom) and 2i (1uM PD0325901 (Axon MedChem) and 3uM CHIR99021 (Axon MedChem)).

METHOD DETAILS

Construction and cloning of FIRE cassettes

DNA oligonucleotides and synthetic gene fragments were obtained from Integrated DNA Technologies (IDT). All constructed plasmids are available on Addgene. All vectors for mammalian cell experiments were purified using ZymoPURE II Plasmid Midiprep kits (Zymo Research). For FIRE1, FIRES-PBCS-CLV3 containing the sensor cassette was constructed, synthesized, and cloned as in Figure 1 schematic. The FIRE1 sensor cassette encodes the fluorescent protein mClover3[43] and sensor composed of ~740 base pair sequence (Figure S1) synthesized based on known mammalian IRP1/2 binding sites.[44,45] FIREC-PBCS-MC2 containing the control cassette was constructed, synthesized, and cloned as in Figure 1 schematic and encodes the fluorescent protein mCherry.[46] For FIRE2, FIRES-PBCS-E670 containing the sensor cassette was constructed, synthesized, and cloned as in Figure 1 schematic. This sensor cassette encodes the fluorescent protein emiRFP670[47] and the FIRE2 sensor is the same as the FIRE1 sensor described above. FIRES-PBCS-MR3 containing the control cassette was constructed, synthesized, and cloned as in Figure 1 schematic. This control cassette encodes the fluorescent protein mRuby3.[43] For FIRE2-FLIP, FIRES-FLIP-PBCS-E670 containing the sensor cassette was constructed, synthesized, and cloned as in Figure 1 schematic. This sensor cassette encodes the fluorescent protein emiRFP670[47] and the FIRE2-FLIP sensor is FIRE1 sensor in backwards orientation. For FIRE2-FLIP, the control cassette is

FIRES-PBCS-MR3. The FIRE sensors used and described in this manuscript are under control of the human phosphoglycerate kinase promoter.

Generation of FIRE ESCs

Transfection of mouse ESCs with the plasmids containing the FIRE sensor and control cassettes and *piggybac* transposase was done using Fugene6 (Promega) 16 h before fluorescence-activated cell sorting (FACS) on a FACSAriaII SORP cytometer (Becton Dickinson) to assay transfected cells by fluorescence and collect preferred clones. Re-analysis and re-sorting of clones was performed within two passages to confirm stable transfection. After plating and selection of single clones and monoclonal culture, final assessment was performed by flow cytometry to confirm FIRE expression in single clones.

Cell culture and embryoid body generation and differentiation

Differential states of mouse ESC pluripotency from naive to Epi-like cell transition were generated by removal of LIF and 2i. In brief, ESCs were plated in ESC medium (as described above). To initiate differentiation, LIF and 2i were removed. Cells were collected at indicated time points following LIF/2i removal. For embryoid body (EB) generation, ESCs were cultured in rotary (100 rpm) suspension culture on a low attachment plate allowing for self-aggregation and regular reproducible spontaneous differentiation over a course of 7–10 days. EB differentiation was evaluated by bulk RNA-sequencing.

Real-time qPCR

RNA was extracted from cells using TRIzol (Invitrogen) and quantified on a Nanodrop spectrophotometer (ThermoFisher Scientific). Reverse transcription and real-time qPCR were performed according to manufacturer's instructions (Maxima, K1641, ThermoScientific; PowerSYBR, Applied Biosystems). qPCR Primer sequences used: mTfrc Forward: AAATTCCCCGTTGTTGAGGC,
Reverse: TGATGACTGAGATGGCGGAA.

RNA-seq library preparation and sequencing

RNA (total or poly-adenylated) was extracted using TRIzol (Invitrogen) or Oligo(dT)25-coated Dynabeads (Invitrogen), respectively. RNA quality was examined by Qubit 2.0 Fluorometer (Life Technologies). cDNA library generation was done using the KAPA RNA Hyperprep kit (KK8541, Roche) following the manufacturer's instructions. cDNA library quality was assessed using Qubit 2.0 fluorometer to determine concentrations. The 4200 TapeStation system (Agilent) was used to determine insert size following the manufacturer's instructions. cDNA libraries were then sequenced using NovaSeq X Systems (Illumina).

Bulk RNA-Seq data pre-processing and analysis

Raw fastq files were filtered and preprocessed by quality trimming using FASTX-Toolkit (http://hannonlab.cshl.edu/fastx_toolkit). Adapters were removed and reads collapsed using unique molecular identifiers using FASTX-Toolkit and Cutadapt (56). RNA-seq read mapping and alignment with alignment to mm10 reference genome assembly was performed using STAR.[48] Read count tables were generated using the RSEM program.[49] Differential gene expression was performed using R packages edgeR[50] and DESeq2.[51] FDR was calculated using the Benjamini–Hochberg method. DE genes were defined with FDR less than 0.05 in comparison to the control group.

Gene ontology and GO enrichment analysis

Gene Ontology reference and GO Enrichment Analysis were accessed and used to perform ontology and fold enrichment analysis using the GO Ontology database https://doi.org/10.5281/zenodo.10536401,[42,52,53]

Flow cytometry

After dissociation into single-cell suspension using Trypsin or TrypLE (ThermoFisher Scientific), cells were resuspended in HBSS/1% BSA and filtered for size by cell strainer (35 micron mesh). Cells were processed by flow cytometry on an LSR II flow cytometer (Becton Dickinson), with events collected by FACS Diva software (BD Biosciences) using a hierarchical gating strategy selecting for a homogeneous cell population (forward-scatter area vs. side-scatter area) of single cells (forward-scatter width vs. forward-scatter area). Dot plots and mean fluorescence intensities for gated events were generated using FlowJo analysis software.

QUANTIFICATION AND STATISTICAL ANALYSIS

No data were excluded from the analyses. Statistical tests were performed in GraphPad Prism (v10). Data collection and analysis were not performed blind to the conditions of the experiments, but data analyses have been performed with identical parameters and software. Data representation and statistical analyses were also performed using R software. The number of biological replicates and independent experiments, both equal to or greater than 3, is indicated in figure legends. The statistical tests used are indicated in the figure legends.